

Study of the Ga doped In(1-x)Ga_xSb(x= 0.10, 0.15, 0.25) crystals' the compositional, structural, electrical, and the microstructures properties: Growth by the VDS-process

D. B. Gadkari*

* Freelance Research & Consultant; Crystal Growth and Technology
Embee-10A, Saibaba Nagar, Borivali (W), Mumbai-400092 India

ABSTRACT

Novel vertical directional solidification process (VDS-process) has been constructed for growth of the III-V detached crystals. Research aim is to grow the gallium ('Ga') doped In(1-x)Ga_xSb(x=0.10, 0.15, 0.25) ingots. The comprehensive characterization of the composition, structure, electrical, microstructure and the thermoelectric properties by tuning the stoichiometry are studied. The doping in pristine InSb decreased the carrier mobility of the binary InSb ingots from $\sim 6.05 \times 10^4 \text{cm}^2/\text{V}\cdot\text{sec}$ to In(1-x)Ga_xSb $\sim 1.241 \times 10^4$, 9.01×10^3 , and $2.436 \times 10^3 \text{cm}^2/\text{V}\cdot\text{sec}$, and the resistivity from $3.0 \times 10^{-3} \Omega\cdot\text{cm}$ marginally reduced to 2.98, 2.58, and $1.69 \times 10^{-3} \Omega\cdot\text{cm}$. Remarkably, the carrier concentration, increased from $\sim 3.8 \times 10^{16} \text{cm}^{-3}$ to ~ 1.89 , 2.29, and $3.15 \times 10^{18} \text{cm}^{-3}$ and increase in dislocation density from $\sim 962 \text{cm}^{-2}$ in to ~ 1.21 , 6.94 and $9.93 \times 10^3 \text{cm}^{-2}$. The 'Ga' doping tailored the band gap of InSb from 0.169eV to 0.2011, 0.2605 and 0.3011eV, and the increased FWHM from 65arcsec InSb to 103, 124 and 145arcsec for the respective growths. The binary InSb perfect single crystal converted to the perfect ternary crystal and decreased XRD peak intensity of the (022) growth direction by doping 'Ga' into InSb. To add, the composition% have been exhibited the point defects and decreased the mobility by one order by doping 'Ga', while the electrical resistivity changes marginally. The carrier concentration increased two fold; it promotes increase in the thermo electric power factor and enhancement in ZT value. The 'Ga' doping forms the second phase of GaSb at the grain boundaries, which reduces the thermal conductivity, increase dislocations, and carrier concentration. The Ga doping, the electron transport enhances, and is potential for the thermoelectric (TE) materials.

Keywords - Directional solidification; X-ray diffraction; Growth from melt Antimonides; Semiconducting ternary compounds; Semiconducting III-V materials

Date of Submission: 05-10-2020

Date of Acceptance: 19-10-2020

I. INTRODUCTION

In(1-x)Ga_xSb crystal band gap can be tuned to the range 0.17 eV (x =0) to 0.72 eV (x =1) by the gallium ('Ga') doping in InSb and useful for the electrical, optoelectronic, micro, thermophotovoltaic, thermoelectric (TE) and IR-devices [1]. III-V crystals are promising materials to replace Si for the next-generation electronics, because of the high carrier mobility [2]. Fast laser operates in the mid-infrared (MWIR 2-5 μm) opened new opportunities for the molecular spectroscopy, medical diagnostics and treatment [3]. InSb and GaSb crystals were grown by dewetting technique. Hall mobility of the dewetted antimonide crystals had the highest values at room temperature (RT) [4]. The intrinsic point defects influence the band structures of the narrow gap GaSb and InSb by doping. Further, the Fermi energies, and the carrier concentration confirms the intrinsic n- and p-type by

anion-rich and anion-poor conditions [5]. Recently, the elements In, Ga, As, Sb are used for growth in Czochralski method for the radiation sensors. Experimentally the highest electron mobility $6.2 \times 10^4 \text{cm}^2/\text{V}\cdot\text{sec}$ is measured for InSb at RT. The each pit density (EPD) was $1.0 \times 10^4 \text{cm}^{-2}$. Raman spectra present two peaks at transversal optical (TO) and longitudinal optical (LO) for InSb, where the first peak is vibrational mode due to the crystalline direction, and second is associated to high defects density [6]. The III-V alloys compounds are important due to a tunable band gap. The Ga_xIn_{1-x}Sb nanowires by the Au seed were grown by metalorganic vapor phase epitaxial (MOVPE) by tuning growth x=1 to ~ 0.3 . In spite of composition % changes, the growth was without change in zinc blende crystal structure [7]. Detached solidification of lightly 'Ga' doped InSb was grown using the ampoule coated with hexagonal boron nitride with the oxide-free material. The temperature increase

with a height of furnace constructed to minimize buoyancy-driven convection. Additionally, the ampoule was backfilled with 20 kPa of Ar-10% H₂ prior to sealing, and no difference in results with freezing rates of 5 and 10 mm/h. The detached portion was depressed from the attached portion was observed [8]. Dewetting growth of GaSb by an oxidising atmosphere in the ampoule was achieved by increase in the wetting and growth angles. Stable dewetting of InSb was not grown, but, the hillocks microstructures were seen. The self-stabilization of the gas pressure was revealed [9]. In(1-x)Ga_xSb films (x = 0 to 1) were deposited by magnetron sputtering on SiO₂/Si substrates. The atomic composition, structure, and electrical properties were tuned stoichiometry of the In(1-x)Ga_xSb films (polycrystalline). The electrical properties by four point and Hall Effect indicated increase in resistivity with 'Ga' concentration [10]. The energy gaps, electron effective masses, and phonon frequencies in InSb spherical quantum dots were in good agreement with the literature. The bulk to nano-scale properties were changed significantly [11]. The 'Ga' substituted in InSb crystals, the Ga doping reduced the lattice thermal conductivity, and optimized the mobility of binary InSb, and the lattice thermal conductivity in In(1-x)Ga_xSb(x=0 to 0.2) as reported. The electron and phonon transport is enhancement and potential for TE by the increased figures of merit (ZT) [12]. The 'Ga' dopant on ZnO thin films annealed to improve the conducting properties. The dopants were ionized and contributed to the conducting process by the rapid thermal and CO₂ laser annealing. 'Ga' dopant plays a favorable role in energy band gap [13]. The GaAsSb epitaxial layers were grown by liquid phase epitaxy (LPE) using Bi in the Sb place, which decreases the Sb incorporation in the layers with increased Bi, and a band gap reduction, was measured in GaAsSb layer. The blue shift of the band gap due to the Bi was occurred, the intensity increases and the full width at half maximum (FWHM) decreases for the Ga-As-Sb-Bi grown layers [14]. A gallium-doped and the reduced graphene oxide (Ga-GrO) material were developed by a metal-organic chemical vapor deposition (MOCVD). A 'Ga' doping in graphene materials was tuned electrical properties [15]. The (111) orientated vertical InSb NWs were grown on GaAs substrate by metal-organic chemical vapor deposition (MOCVD) [16]. Raman spectra at RT, the appearances of GaSb-SiO₂ composite film have a larger red shift than that of bulk GaSb because the stress affect thermal expansion and lattice mismatch between GaSb and SiO₂ [17]. InSb crystals are not promising thermoelectric due to the high thermal conductivity. But, Ga doping and nano-inclusions

acts as phonon scattering centers, contribute to the weak influenced electrical transport and reduced lattice thermal conductivity (κ_L). The In_{0.9}Ga_{0.1}Sb has the perspective at intermediate temperatures as the κ_L decreased and the ZT increased [18]. Thermoelectric power requires crystals to control phonon and free charge carrier transport properties. The control on lattice vibration, structural imperfections and defects engineering (point defects, segregations) has the effect on electron and phonon transport properties. The ternary alloy In(1-x)Ga_xSb improved by the point defects and compositional segregations. The point defects affected the electrical resistivity, and Seebeck coefficient due to carrier concentration; while ZT of In_{0.95}Ga_{0.05}Sb enhances by the point defects and compositional segregations [19]. In(1-x)Ga_xSb(x = 0 to 1) was grown by solidification process. Raman measurement showed the optical modes of phonon vibrations in binary InSb and GaSb, suppressed in ternary In(1-x)Ga_xSb. The phonon vibrations have been scattered effectively by the defects, which reduced lattice thermal conductivity. The thermal conductivity of binary InSb and GaSb drastically reduces in In(1-x)Ga_xSb by scattering. It results the highest ZT, because of its higher power factor, and the higher ZT in In_{0.8}Ga_{0.2}Sb [20]. The n-type In_{0.8+y}Ga_{0.2}Sb(y = 0 to 0.06) ternary crystal grown by Spark sintering (SPS) method, two phases were observed the major InSb-rich phase and minor GaSb-rich phase. The increasing In content increased the Seebeck coefficient of In_{0.8}Ga_{0.2}Sb. Ga alloying reduces the lattice thermal conductivity, the (In, Ga)Sb based TE materials proposed for the intermediate temperatures [21]. The distribution of GaSb nano-inclusions by 'Ga' doped and Sb rich forms the second phase of GaSb at grain boundaries, reduces the thermal conductivity. The doping increase carrier concentration, and suppresses the bipolar effect and enhance in power factor [22]. Highly mismatched alloys (HMAs) modify the electronic band structures developing high-performance thermoelectric materials. GaBi_{1-x}Sb_x (HMAs) is potential for thermoelectric applications. The increase in Seebeck coefficient and decrease in the electrical conductivity of GaBi_{1-x}Sb_x alloy as a function of Sb displayed large thermoelectric power factor and the figure of merit ZT [23]. The p-type Ge_{0.9}Sb_{0.1}Te (1+X) by melt spinning method with hot pressing (MS-HP) grown. Enhancement thermoelectric properties increased Seebeck coefficients and reduced thermal conductivities. The microstructures reduce thermal conductivities by the Ge precipitates, twin, nano-inclusion [24]. Intrinsic AlSb has a high resistivity and the lattice thermal conductivity result the ZT value low. Inclusion and dispersion in AlSb has reduced the thermal

conductivity with improved electrical conductivity without decrease in thermo-power [25]. The EPD was low and the growth rate was higher in the microgravity (μg) [26]. The $\text{In}_{0.11}\text{Ga}_{0.89}\text{Sb}$ crystal was grown in the space. The non-steady state equilibrium in the melt was achieved in μg . The compositional homogeneity and uniformity by a higher growth rate was achieved [27,28]. The interface shape was nearly flat in μg , whereas in 1g was highly concave with facets at the edge. The EPD was low and the growth rate was higher in μg [29]. The shape of solid-liquid interfaces and composition was affected in 1g condition [30]. The microstructure, the convection, and solute transport was affected by gravity, the grain sizes were small in 1g. The solidification velocities of crystal were rapid and low influence on microstructure in μg . The μg conditions were promoted the detached growth. The process was controlled by thermal diffusion, hydrostatic pressure and wall effect [31,32].

The entire detached III-V crystal growth has suppressed the buoyancy convection, and hydrostatic pressure; whereas there is no major change of the composition %, and the macroscopic segregation. The entire detached crystals quality depends on the gradients, the source materials, pressure difference, and the growth rate. Grown crystals qualities enhanced due to the decreased native defects and dislocations by increasing crystallization using VDS-process. The results have been published elsewhere [33-47].

In this manuscript first time, the entire detached $\text{In}_{(1-x)}\text{Ga}_x\text{Sb}$ ($x=0.10, 0.15, 0.25$) crystals grown by VDS-process. The compositional %, structural, electric, growth morphology and Thermoelectric (TE) properties of entire detached $\text{In}_{(1-x)}\text{Ga}_x\text{Sb}$ crystals are investigated. The point defects and compositional segregations are analyzed. The 'Ga' dopant in detached InSb crystal, and composition in $\text{In}_{(1-x)}\text{Ga}_x\text{Sb}$ and the effect on properties are reported.

2. EXPERIMENT

2.1. The crystal growth initial steps

The experimental crystal growth procedure of the Ga doped $\text{In}_{(1-x)}\text{Ga}_x\text{Sb}$ ($x<0.3$) crystals is similar as applied the uniform procedure in the III-V detached crystals [44-46].

Three $\text{In}_{(1-x)}\text{Ga}_x\text{Sb}$ (0.10, 0.15, 0.25) entire detached ingots grown by the VDS-process. The prior to sealing, one side conical ampoule was cleaned by the high temperature flame. The oxygen, nitrogen and contaminations from the stoichiometric In, Ga, Sb source materials was eliminated Table-1. A quartz ampoule with vacuum $\sim 1.3 \times 10^{-3} \text{Pa}$ was refilled by pure argon gas, and the source materials

purged alternately 10 times. Finally, these materials, and ampoule backfilled pure argon pressure 20-30KPa was sealed. This ampoule is positioned vertically in the VDS furnace Fig-1a. A conical tip angle of an ampoule was constructed of the $\sim 45^\circ$ to $\sim 75^\circ$, diameter 10-22mm, and length ~ 60 -75mm. Entire detached binary InSb and GaSb perfect single crystal growth and properties were published elsewhere [33-46]. However, the conical tip possibly promotes the detached growth and reduces the defects. In detached growths, the self-growth of seed and self-stabilization of pressure difference perhaps developed. A vertical furnace with increasing temperature from bottom to the center was applied to grow $\text{In}_{(1-x)}\text{Ga}_x\text{Sb}$ detached crystals by VDS-process, Fig-1. The temperature increasing with a height of furnace constructed to minimize buoyancy-driven convection [8]. Briefly procedure repeated here, the vertical furnace temperature profile Fig-1b,c. In this figure, Red-L: a line of the liquidus, Red-S: a line of the solidus (original furnace profile Fig-a), and Black-x: the growth composition %. The growth is below the center of furnace at higher gradients, and then the L-S curves never meet Fig-1c. At the low temperature gradient, the L-S curve meet at point 'C' (crystallization), i.e. the L, S, and x meets at point 'C'. The high temperature gradients (axis) gradually reduce to low, and then crystal always grows at the low temperature zone Fig-1c. At C/M interface, the solidification changes from the m.p. 525°C (InSb) to 712°C (GaSb) in the upward direction (fixed set temperature $\sim 760^\circ\text{C}$). The ampoule downward velocity 'v' has a high growth rate. The phase changes, heat transfer, fluid flows, and solute transport affect the solidification process. always grows at the low temperature zone Fig-1c. At C/M interface, the solidification changes from the m.p. 525°C (InSb) to 712°C (GaSb) in the upward direction (fixed set temperature $\sim 760^\circ\text{C}$). The ampoule downward velocity 'v' has a high growth rate. The phase changes, heat transfer, fluid flows, and solute transport affect the solidification process

2.1 The entire detached growth

The vertical furnace profile is shown in Fig-1a. The previous VDS experiments growth process is in [33-47]. Three $\text{In}_{(1-x)}\text{Ga}_x\text{Sb}$ crystals grown by the VDS-process, however, the brief procedure is here as the seven steps: i) the furnace temperature raised to $\sim 8500\text{C}$ in 3h (overheating condition 150°C) to melt the source materials in a heat zone $T_{\text{Centre}} > T_{\text{mp}} > T_{\text{Bottom}}$, for complete-congruent melting of the source materials, then kept for 3h. The vertically ampoule with melt is rotated continuously 10rpm rate. An ampoule used for ingot growth contained melt is rotated (stirred) at the 10

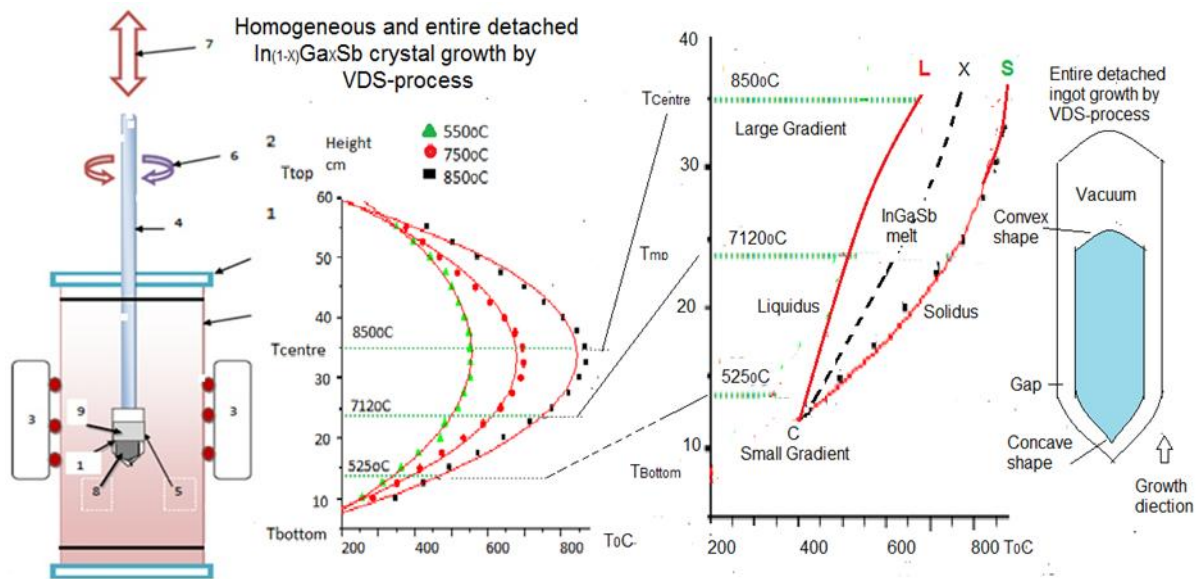


Figure- 1 The schematic diagram of the VDS process a: the numbers in 1a, the quartz growth chamber, 2) Wilson seals, 3) a vertical furnace with the thermocouples (red circles), 4) a vertical shaft to hold the ampoule at the centre of furnace, 5) a vacuum sealed quartz ampoule, 6) a clockwise and anti-clockwise rotation 7) the up and down movement of an ampoule, 8) as grown detached ingot inside ampoule, 9) the vacuum (open space) above a melt, 10) the vacuum sealed quartz ampoule with source materials inside, 11) The open quartz tube covered with silicon wool, 12) The bottom Wilson seal was removed and exposed to ambient temperature. b) The temperature profile of furnace used for melt solidification. The height of furnace 66cm, and the hot zone of furnace at the centre 33cm. Below, towards bottom side the ingot process carried out, c) In VDS-process, the radial gradients is $1.4^{\circ}\text{C}/\text{cm}$ and the axial gradient decreases towards lower temperature from large gradient condition ($32^{\circ}\text{C}/\text{cm}$) to small gradient condition ($12^{\circ}\text{C}/\text{cm}$). The red-L was the line of liquidus, green-S was the line of solidus, and black 'x' was the region of the Ga-In-Sb composition % along the growth direction. d) The schematic as grown entire detached crystal (light blue colour) with a gap between the inner ampoule wall and as grown ingot.

rpm clock-wise and anticlock-wise mechanism for the mixing of Ga, In, Sb source materials. The actual calibrated furnace profile is in Fig-1b. ii) The vertical ampoule containing congruent melt is translated downward to the fixed set temperature $\sim 765^{\circ}\text{C}$ (overheating condition 50°C) by the lowering rate $10\text{mm}/\text{h}$ in 3h. Consequently, the C/M interface changes from m.p. of InSb to GaSb (525°C to 712°C) during solidification process of the $\text{In}(1-x)\text{Ga}x\text{Sb}$ ingot in a heat zone $T_{\text{Centre}} > T_{\text{mp}} > T_{\text{Bottom}}$. The enlarge temperature profile is shown in Fig-1c. iii) For the homogeneous and chemically uniform melt, the steady isotherm is maintained for 3h. iv) Ingot growth process: An ampoule of the homogeneous and congruent melt has translated downward for the solidification by the freezing rate $\leq 5\mu\text{m}/\text{s}$ ($1.38\mu\text{m}/\text{s}$) in the heat zone from the large axial gradient ($32^{\circ}\text{C}/\text{cm}$) towards the small axial gradient ($12^{\circ}\text{C}/\text{cm}$). Where actual crystallization / solidification begins is shown in enlarge profile Fig-1c. The radial gradient constant is maintained at $1.40\text{C}/\text{cm}$. The crystallization (solidification) of the ingots lengths ($\sim 50\text{-}75\text{mm}$) and taking out the length 100mm of ampoule from the heat zone, time is

$\sim 20\text{h}$. The identical growth rate for the three ingots are $\sim 5\text{mm}/\text{h}$, details is given in [46]. The temperature gradients in the growth chamber of the vertical furnace were calibrated by the vertical and horizontal temperature profile of a furnace by thermocouples Fig-1a. The ampoule lowering growth rate $10\text{mm}/\text{h}$ was calculated from our initial experiments using smooth quartz ampoule thermodynamical condition [47]. v) The grown $\text{In}(1-x)\text{Ga}x\text{Sb}$ ingot is lowered $10\text{mm}/\text{h}$ for the 3h to move below 100°C the m.p InSb (lower cooling condition), then, kept for 3h. vi) then here, the temperature attained to 3000C (the stabilizing temperature condition), kept for 2h. vii) Finally, the furnace switched off for a natural cooling then waited for 2h to cool as grown ingot. Entire detached growth time was 45h, and the time including the growth arrangement before heating and taking out ingot was 3h. Total growth process time was 48h. The schematic detached ingot is shown in Fig-1d. The ingot came out easily by tapping the ampoule. The $\text{In}(1-x)\text{Ga}x\text{Sb}$ ingots diameters 10 to 14mm and lengths $\sim 50\text{-}75\text{mm}$ is shown in Fig-2. While, excessive heat conduction of the ingot was



Figure-2 The as grown ingots of $\text{In}_{(1-x)}\text{Ga}_x\text{Sb}$, a) IGS-1 ($x=0.1$), b) IGS-2 ($x=0.15$), c) IGS-3 ($x=0.25$). The surfaces are without growth morphology, at the beginning concave and the end growth convex..

prevented hanging the ampoule by a shaft as in Fig-1a. The ampoule not having downward support was prevented heat conduction $\text{In}_{0.11}\text{Ga}_{0.89}\text{Sb}$ crystal was grown in space, and the composition uniformity achieved by a. higher growth rate in microgravity (μg) [26-28]. Non-steady state equilibrium in the melt composition promoted the compositional homogeneity of $\text{Ga}_{1-x}\text{In}_x\text{Sb}$ in μg [29]. The nearly flat shape of the interface was formed in μg for the higher growth rate. The crystal quality was better in μg . The shape of interfaces affected in 1g. The solidification velocity of crystal rapid and low influence on microstructure was in μg . The μg conditions promoted the detached growth [30-32].

2.3 The substrates preparation

The substrates preparation process was similar [44-46], thus the grown ingots sliced the thickness $\sim 500\mu\text{m}$, the laterally and longitudinal with the preferentially (022) growth direction. The substrates were cleaned mechanically by the grinding, lapping with carborundum ($5\mu\text{m}$) power and polished to the mirror finish by an alumina abrasive (0.1 and $0.03\mu\text{m}$) powder. The substrate of the detached ingot exhibited the mirror shining by lesser time compare to the attached ingot. The substrates were cleaned in the warm TCE, acetone

and methanol of electronic grade. The substrate dimensions were $10 \times 10 \times 0.5\text{mm}^3$. At the four corners of substrate contacts were made in van der Pauw geometry for alloying the indium (In) balls at 2000C for 30 seconds in flowing a high purity H_2 for the analysis and characterization. 2.4 Characterizations methods

The equipment's are similar as in [44-46]. The substrate from $\text{Ga}_{(1-x)}\text{In}_x\text{Sb}$ were sliced to characterize. The measurements were at the room temperature (RT): i) The substrates cut as specified dimensions by Buchler ISOMAT Low speed saw and diamond cutter (Low Speed Saw and Metacut-DC-I). ii) The mirror finishes of the substrate prepared by Metapol DC-II. iii) The development of growth morphology by the selective chemical etching CP4, and modified CP4. iv) The dislocation density (dd) measured by the Metallurgical microscope (Carl Zeiss, Karl Suss MJB-3, Metagraph-I Metatake), and Interface contrast microscopy (Nomarsky) by Leitz Arisomet vaviport wild 46. v) The investigation structures of substrate by X-ray diffraction (JEOL JDX8030, SIEMENS Krystalloflex diffractometer) using $\text{CuK}\alpha$ radiation, $\lambda=1.504\text{\AA}$, Laue spectrometer (Huber) was applied for the single crystal growth and orientation study. Scanning electron microscopy SEM (JEOL JSM-840) used for the microstructures

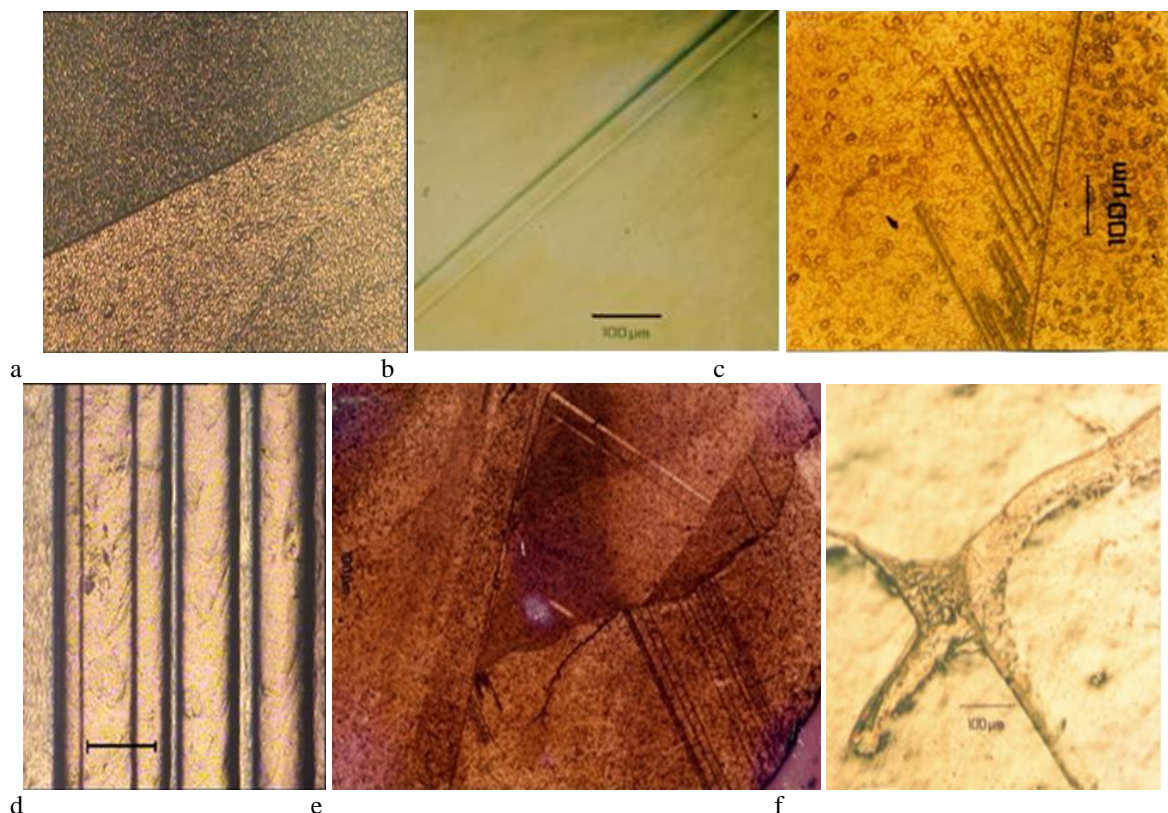


Figure-3 The growth morphology, a) a low energy plane of the twin lamella, b) a twin lamellae, c) a line growth with the Sb bands d) Energy optimization by multi twin lamellae on a plane, e) the three large size grain growths on the substrate surface, f) the Sb eutectic growth.

characterizing. vi) Composition % 'x' determined by EDAX (Analer Kevex). vii) Hall measurement by Four probe CTI closed cycle Liquid helium crystal model No M22 with Keithley-220-current sources, 182-nonovoltmeter. viii) Energy gap 'Eg' measured by FTIR (Perkin-Elmer-GX), Spectrum-65, Biorad-45, IR measurement by ISS 88. x) Microhardness measured by Vickers test by (MVH-I Metatak). I.

RESULTS AND DISCUSSION

3.1 Ingots surface features

The grown ingots surface features of $\text{In}(1-x)\text{Ga}x\text{Sb}$ are shown in Fig-2. The ingots have the concave shape in the beginning growth due to shape of the melt drop, and the convex or solid drop shape at the end growth. These entire detached ingots growths have lower smoothness and shiny surface compared to the ingots in [44-46] as the 'Ga' doping in InSb probably introduced the native defects, vacancy and microstructures. Growth converted the perfect single growth (binary InSb) to perfect ternary $\text{In}(1-x)\text{Ga}x\text{Sb}$ crystals. This could be by the higher growth rate of ingot at the solidification point was resulted perfect $\text{In}(1-x)\text{Ga}x\text{Sb}$ crystal growth. It reveals the presence of segregation near interface, form non-uniform composition. Resulted decrease in homogenous growth by the non-planner and zig-zag (hazy) interface shape. The 'Ga' doping may increase

the native defects in the crystal by increasing the dislocation density, thus, the lower crystallizations as in [44-46].

3.2 Growth morphology

Three $\text{In}(1-x)\text{Ga}x\text{Sb}$ pseudo binary and highly miscible alloy crystals grown by the entire detached phenomenon using VDS-process Fig-2. The experiments result have indicated that the increase in 'Ga' doping increases the marginally segregation, native defects, the microstructures and the dislocation density. The measured dislocations density of the three ingots are increased from $0.96 \times 10^3 \text{cm}^{-2}$ (InSb), to i) $1.239 \times 10^3 \text{cm}^{-2}$, iii) $4.1 \times 10^3 \text{cm}^{-2}$, and iii) $5.72 \times 10^3 \text{cm}^{-2}$, i.e. 10^3 to 10^4cm^{-2} range. The melt rotated (stirring) during synthesis of the $\text{In}(1-x)\text{Ga}x\text{Sb}$ crystal growth using controlled VDS-process. The crystals transverse distribution and transport properties of the $\text{In}(1-x)\text{Ga}x\text{Sb}$ grown crystals is shown in Table-2,5. As the gallium distribution was no major fluctuations, hence, the electrical and transport properties were contributing to increased lattice hardness. The low angle twin lamella ($<15^\circ$) growth of first two growth ($x=0.10, 0.15$) is shown in Fig-3a,b,c, and the multi twin lamellae, the grain boundaries, and the eutectic

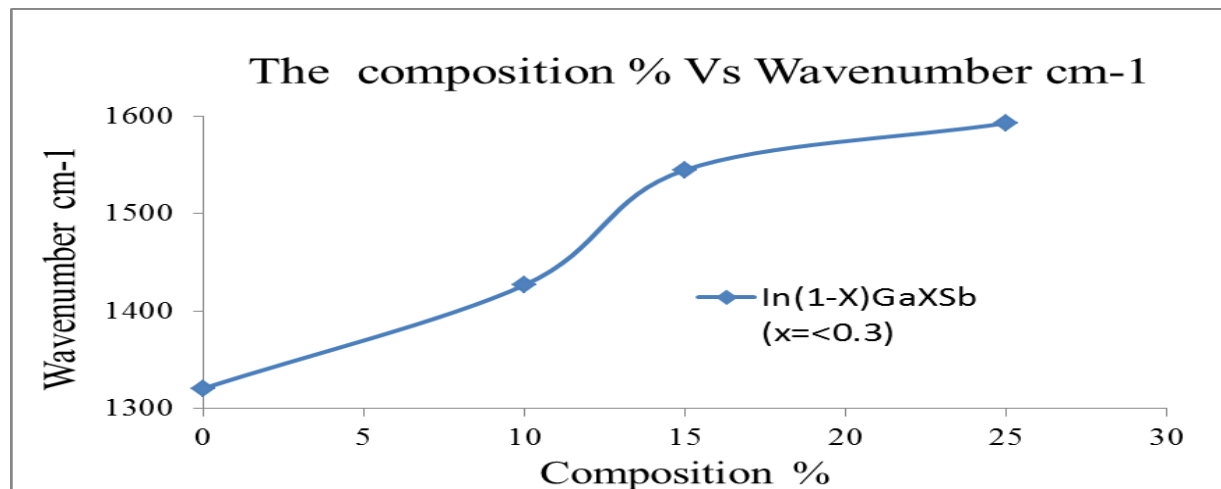


Figure-4 the graph of composition Vs wavenumber

growth by the second growth ($x=0-25$) is shown in Fig-3d,e,f. The twin lamella growth is assumed as the perfect crystal growth. A coherent twin boundary is the high degree of perfect single crystal in binary InSb and GaSb. The perfect crystal of the ternary $\text{In}(1-x)\text{Ga}x\text{Sb}$ growths are the oriented single line growth of the twin lamella presented in Fig-3a,b and the impurity bands growth close to twin lamella in Fig-3c. Growth morphology of third growth is in Fig-3d,e,f as the second phase growth by grain boundaries, similar in [22]. The large three grain boundary, the twin lamella growth on first grain (clockwise) is shown in Fig-3d. The parallel impurity (Sb) bands on second grain are shown in Fig-3d. The third grain shows the slightly vertically inclined twin lamella growth in Fig-3e. The eutectic star-like micro growth of antimony (Sb) in Fig-3f, it demonstrates the The perfect single crystal InSb growth by VDS-process, wavelength number cm^{-1} is 1321 and the $E_g=0.165\text{eV}$ complicated melt flows patterns at C/M interface before solidification. The eutectic growth has large area at center, then, it is narrowed towards the away from the edge (periphery) of the substrate. The oriented two grains together at the boundary plane by the low angle boundaries angle ($<15^\circ$) are a plane mirror images in Fig-3. Thus, the twin lamella

grows by a single plane of atoms favors the coherent twin boundaries crystals. Which is internal structure formed by its a mirror image along the shared border. It confirms the symmetric interface with a perfect crystal; hence, other is the appearances of its mirror image. Because, the shape of C/M interface during the crystal growth can be slightly convex by the thermal stress. The dislocation density increased from 10^3cm^{-2} to 10^4cm^{-2} reveals the increased defects by 'Ga' doping in detached $\text{In}(1-x)\text{In}x\text{Sb}$ crystals. The 'Ga' doping increases the thermal stress by the increased dislocation density, and defects such as the twin lamella, oriented grain boundaries, segregation, inclusions, etc. in a perfect single by the entire detached InSb crystals [33-46]. The lower quality of the $\text{In}(1-x)\text{Ga}x\text{Sb}$ ingots because of - i) the constitutional supercooling (CSC) lead to a segregation (eutectic growth). ii) The twins, grain and micro-inclusions, dislocation density and defects by a thermal stress. The 'Ga' substitution and micro inclusions could be the centers of the phonon scattering. It infers the defects and inhomogeneous crystal structure contribute to the weak influence on electrical transport to reduce the lattice thermal conductivity (κ_L). No smaller grains as well as the

Table-1 For In(1-x)Ga_xSbVDS experiments, the stoichiometry of source materials for the growth of In(1-x)Ga_xSb. The starting masses of the In, Ga and Sb are in this table.

Sr No.	Target alloys	mass In (gm)	mass Ga (gm)	mass Sb (gm)	Total mass gm In(1-x)Ga _x Sb
1	In 0.9Ga0.10Sb	8.4889	0.5727	10.00	19.0615
2	In 0.85Ga0.15Sb	8.0160	0.8590	10.00	18.8750
3	In 0.75Ga0.25Sb	7.0730	1.4320	10.00	18.5050

Table-2 the composition % of three Ga_(1-x)In_xSb (x<0.3) ingots measurement by EDAX

Substrate		InGaSb-1 x=0.1			InGaSb 2 x=0.15			InGaSb -3 x=0.25		
No.	L cm	In	Ga	Sb	In	Ga	Sb	In	Ga	Sb
1	1	46.72	4.94	48.35	44.20	7.90	44.20	39.85	11.9	44.87
2	1.5	44.41	6.47	49.12	46.22	4.91	46.22	38.64	11.6	45.86
3	2	47.49	4.34	48.17	43.84	6.79	43.84	40.21	11.7	45.21
4	2.5	49.89	2.74	47.37	43.64	7.35	43.64	42.09	12.2	45.81
5	3	42.04	10.69	47.27	45.53	6.22	45.53	41.91	12.5	44.61
6	3.5	46.60	4.28	49.11	43.17	6.46	43.17	42.61	13.5	46.69
7	4	46.08	4.32	50.69	25.61	22.12	25.61	43.96	14.2	45.92
8	4.5	42.51	4.86	49.63	32.25	15.69	32.25	43.49	14.6	45.01
9	5	48.82	3.85	47.31	32.46	16.03	32.46	43.16	15.5	45.83
10	5.5	46.09	4.82	49.11	35.52	13.86	35.52	42.8	15.3	45.33
11	6	48.08	4.32	47.60	39.09	10.41	39.09	42.72	15.9	44.87
12	6.5	44.82	4.86	50.33	41.20	9.59	41.20	43.64	15.6	45.86

Table-3 Infrared measurement of the In(1-x)Ga_xSb crystals at 300K

Subst No.	Ga _(1-x) In _x Sb-1 (X=0.10)			Ga _(1-x) In _x Sb-2 (X=0.15)			Ga _(1-x) In _x Sb-3 (X=0.25)		
	W /cm	λμm	Eg eV	W /cm	λμm	Eg eV	W /cm	λμm	Eg eV
1	1361	7.3475	0.1687	1421	7.0373	0.1762	1479	6.7613	0.1834
3	1392	7.1787	0.1727	1507	6.6357	0.1884	1519	6.5832	0.1883
5	1401	7.1327	0.1738	1521	6.5746	0.189	1561	6.4021	0.1937
7	1427	7.0077	0.1769	1545	6.4725	0.192	1593	6.2774	0.1975
9	1467	6.8166	0.1819	1663	6.0132	0.206	1673	5.9772	0.2075
11	1485	6.7340	0.1841	1695	5.8997	0.210	1737	5.7570	0.2154
13	1563	6.3979	0.1938	2042	4.8972	0.2532	2267	4.4111	0.2811
15	1621	6.1690	0.2011	2101	4.7596	0.2605	2428	4.1186	0.3011

cracks due to the native acceptor defects and the micro-structural growth was compensated by 'Ga' dopant. The lattice defects and the second phase formed by the GaSb at grain boundaries Fig-3d,e,f. The GaSb second phases reduce the thermal conductivity, then it increases the carrier concentration suppresses the bipolar effect of grown crystals, which enhances the power factor. Table-5. The doping induces fluctuation by decreasing the lattice thermal conductivity, also reported in [22]. The microstructures such as twins and micro growth contribute to the reduction in thermal conductivities with the high power factor and ZT [25, 29]. There are various methods to reduce the lattice thermal conductivity by the phonon scattering such as the point defects, dislocations, micro structuring [25].

The faster solidification velocity of the crystal, the small microstructure growth was suppressed. It was controlled by thermal diffusion, hydrostatic pressure and wall effect, and the higher growth rate in μg. [27-33]. an entire detached crystal growth by VDS-process is close to the detached crystal growth in space.

Vickers micro-hardness indentations test, the binary InSb Hv=2.21GPa. The three ingots, the hardness is for In_{0.9}Ga_{0.1}Sb= 2.26GPa, In_{0.85}Ga_{0.15}Sb= 2.29GPa, In_{0.75}Ga_{0.25}Sb= 3.13GPa. The hardness (Hv) attributed to the crystal perfection and the dislocation density (dd). The extremely high order strength crystal structure reveals the perfect single crystals for dd < 10³cm⁻². The perfect crystal showed range 10³cm⁻² to

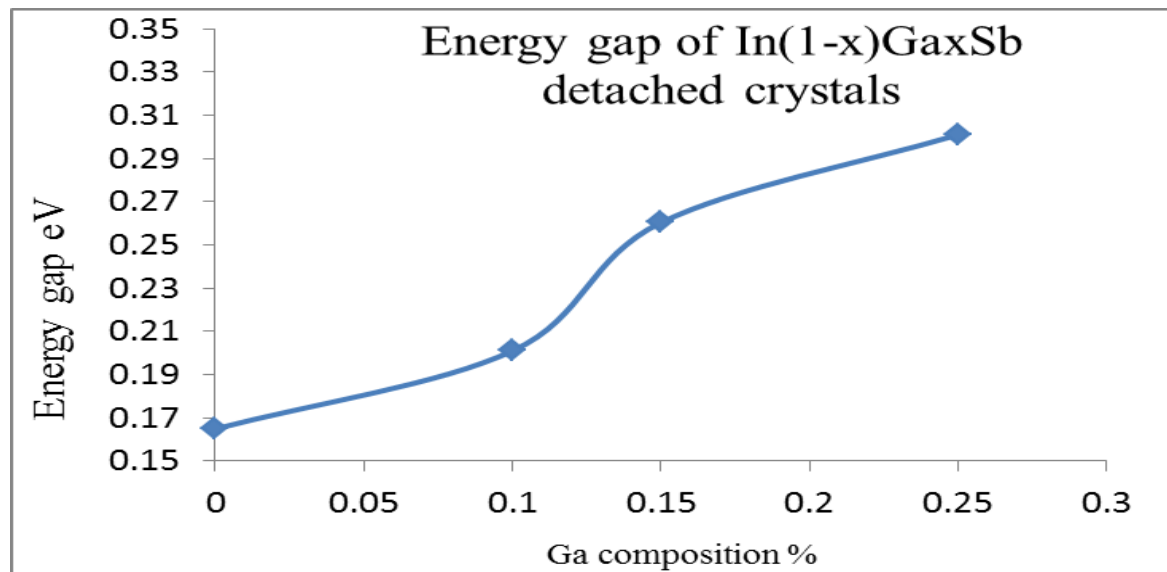


Figure-5 Ga composition 5% Vs Energy gap

10^4cm^{-2} , because, the hardness increase by the dislocation-dislocation motion. The hardness decreases with increase in dislocation density for $dd > 10^4 \text{cm}^{-2}$ by a motion of dislocation energy (44-46).

3.3 The composition analysis

The substrates were selected from the ingots body of the three entire detached $\text{In}(1-x)\text{Ga}_x\text{Sb}$ ($x < 0.3$) ingots for the composition analysis. The In, Ga Sb elements composition % distribution profiles is in Table-2. The crystal growth by VDS-process existed by the diffusion at the axisymmetric temperature distribution, thus the segregation coefficient of the 'Ga' composition may be $k < C_s/C_l < 1$. The 'Ga' concentration nearly uniform along the preferred (022) growth direction, hence predicted the perfect crystal growth by entire detached $\text{In}(1-x)\text{Ga}_x\text{Sb}$. These ingots growth's parameters and conditions are similar in [44-46]. The minor differences in composition % correspond to specifically the highly sensitive entire detached process. The composition % content analysis of the three ingots is possibly the single-phase growths.

A) $\text{In}(1-x)\text{Ga}_x\text{Sb}$ -1 ($x=0.10$) ~ $L=65\text{mm}$. ii) The actual stoichiometric Wtgms is: In- 8.4889, Ga- 0.5727, Sb- 10.00, Table-1. iii) Actual 'Ga' stoichiometric Wtgms is 0.5727gms, the 'Ga' concentration changes is 0.0096 (0.010) mole% per mm along the growth direction. iv) Actual 'Ga' stoichiometric Wtgms of substrate-6 at 35mm is 0.336ms. v) From Table-2, the composition % of substrate-6 is: In- 46.60%, Ga- 4.28%, Sb- 49.11%. vi) The Wtgms of Ga 10% was 0.5727gms for $L=65\text{mm}$, whereas the Ga% is 4.28% at 35mm, its Wtgms was 0.2451gms, thus, the 'Ga' concentration

variation of $L=35\text{mm}$ was 0.007mole % per mm of the substrate-6. vii) The 0.007mole % per mm decreased from 0.0096mole % per mm. The lesser 'Ga' atoms incorporated into InSb matrix, thus the substrate is n-type conductivity with two fold increase in carrier concentration due to the native defects Table-5. viii) Wtgms of 'Ga'; is 0.5727gms for 0.10gms, then for 0.2451gms is 0.0421gms (~0.04gms) ix) The composition % converted in Wtgms, $\text{In}(1-x)\text{Ga}_x\text{Sb}$ -1, substrate-6 is $\text{Ga}_{0.96}\text{In}_{0.04}\text{Sb}$. Its mobility is $\mu=9.57 \times 10^3 \text{cm}^2/\text{V}\cdot\text{sec}$, resistivity $\rho=5.14 \times 10^{-3} \Omega\cdot\text{cm}$, and $n=1.27 \times 10^{18} \text{cm}^{-3}$. $\text{Ga}_{0.96}\text{In}_{0.04}\text{Sb}$ growth is n-type conductivity due to the presence of native defects. The 'Sb' vacancies increased by 'Ga' doping, which decreased the carrier mobility and increased the carrier concentration by increasing native defects [22-25]. For other two ingots $\text{In}(1-x)\text{Ga}_x\text{Sb}$ -2 ($x=0.15$) and $\text{In}(1-x)\text{Ga}_x\text{Sb}$ -3 ($x=0.25$), similar procedure can be applied.

B) $\text{In}(1-x)\text{Ga}_x\text{Sb}$ -2 ($x=0.15$), and $\text{Ga}_{0.85}\text{In}_{0.15}\text{Sb}$ -2-5, explanation similar as in A), the mobility $\mu=4128 \text{cm}^2/\text{V}\cdot\text{sec}$, resistivity $\rho=1.34 \times 10^{-3} \Omega\cdot\text{cm}$ is in Table-5. Growth is n-type conductivity due to the increase in native defects.

C) $\text{In}(1-x)\text{Ga}_x\text{Sb}$ -3 ($x=0.25$), $\text{Ga}_{0.75}\text{In}_{0.25}\text{Sb}$ -2-4, the mobility $\mu=718 \text{cm}^2/\text{V}\cdot\text{sec}$, resistivity $\rho=3.10 \times 10^{-3} \Omega\cdot\text{cm}$ is in Table-5. The mobility and carrier concentration differs from the (A) and (B) interpretation. The decrease in mobility, and increases carrier concentration is due to increase in the 'Ga' doping, then point defects also increases, hence the charge carrier's increase. However, the mobility converts from n-type (electron) to p-type (hole); whereas the carriers' concentration is low orders as of A and B.

Table-4 XRD Measurements of the In(1-x)Ga_xSb-1:

In(1-x)Ga _x Sb 1-3		In(1-x)Ga _x Sb 1-8		In(1-x)Ga _x Sb 1- 13		In(1-x)Ga _x Sb 1- 18		In(1-x)Ga _x Sb 1- 22	
2 Θ	d	2 Θ	d	2 Θ	d	2 Θ	d	2 Θ	d
23.78	3.739	23.88	3.723	23.98	3.708	23.76	3.742	23.80	3.736
24.42	3.642	24.26	3.666	24.86	3.579	24.50	3.630	24.02	3.702
39.32	2.288	39.31	2.286	39.34	2.287	39.36	2.287	39.36	2.284
40.19	2.251	40.10	2.247	40.14	2.245	46.50	1.951	41.28	2.181
41.22	2.189	41.26	2.186	41.22	2.188	71.32	1.321	41.41	2.178
41.32	2.183	47.76	1.903	41.38	2.180	71.68	1.316	39.36	2.284
48.54	1.874	48.36	1.881	48.56	1.873	76.40	1.311	39.78	2.264
71.70	1.315	59.12	1.561	48.96	1.859	23.76	1.239	40.32	2.235

The crystal data of this table are used to compare with the standard diffraction data of the InSb with experimental larger height peak (022), ASTM (JCPDS) card number 6-0208, for the standard diffracted angle $2\Theta=39.3095$, lattice distance $d=2.290\text{\AA}$, Miller indices $h\ k\ l=022$, and lattice constant $a=6.4782\text{\AA}$. We have used the corresponding data of this table (Italic numbers highlighted in black) for the explanation. The 'd' values decreases and FWHM increase thus the InSb perfect single crystal converted into perfect

The electric analysis of the ingots showed that the 'Ga' composition % <0.2 is good for TE application as the mobility decreased and concentration increased, which increases the the power factor and hence ZT. This is due to the presence of the low angle grain boundary, eutectic growth, growth morphology and segregation. The 'Ga' increases point defects, thus the lattice hardness and the carrier concentration increases, while the carrier mobility optimized as the native defects increases. It decreases the lattice thermal conductivity and increasing the power factor [12,22-25],and the growth had higher growth by VDS-process. The three ingots' substrate position, wavenumber, wavelength and 'Eg' is in Table-3, the composition% 'x' versus wavenumber is shown in Fig-4. The infrared transmission % reduced. The engineering of band gap attributes the as Ga doping in InSb increases correspondingly ternary In(1-x)Ga_xSb energy gaps also increases, because, Ga introduces native defects (vacancy and antisites). The energy gap ranges are in Table-3, for i) In(1-x)Ga_xSb-1(x=0.10) is 0.169eV to 0.201eV, ii) In(1-x)Ga_xSb-2(x=0.15) is 0.176eV to 0.261eV, iii) In(1-x)Ga_xSb-3(x=0.25) is 0.183eV to 0.301eV. Band gap and wavelength changes potential for the LWIR [1-3], MIDIR devices [3] and the thermoelectric (TE) materials [12,18-25].

3.4 The structural analysis

XRD powder diffraction measurements of the three In(1-x)Ga_xSbingots is in Table-4. The standard ASTM/ JCPDS card No. 06-0208 (InSb) compared with the diffraction measurements (Italic highlighted black numbers), which are displayed the new peak position. The highest diffraction peak (220) is

highlight the growth direction, and three ingots growth exhibit the similar diffraction peaks with a shift in diffraction angle with increasing Ga doping is shown in Table-4. The peaks 2 Θ and the lattice distance 'd' indicates the red-shift toward higher angle from the standard $2\Theta=39.3095$ (InSb), similar is also reported in [10,12-15,22-25]. A larger red shift of the In(1-x)Ga_xSb crystals is the displacement in angle correspondences to the increasing Ga doping concentration; the lattice parameter decrease due to the shorter atomic distances of the Ga-Sb bonds compared to those of the In-Sb bonds in the In(1-x)Ga_xSb crystals. The broadening of peaks relates to the lattice strain due to the crystal imperfection and distortion, because the stress affect thermal expansion and lattice mismatch between InSb and GaSb. The 'd' value decreased from lattice distance $d=2.290\text{\AA}$ (InSb card No. 06-0208) due to the smaller ion radius of 'Ga'. It confirms that 'Ga' was successfully incorporated into the crystal lattice of the three In(1-x)Ga_xSb crystals. Further, the broad peak reveals the reduced crystallization after 'Ga' doping in InSb matrix. However, the entire detached ternary ingots showed the zinc blend crystal structure, similar to binary InSb crystal after 'Ga' doping by forming In-Ga-Sb matrix structure. The preferential sharp (022) peak is within the InSb card number 06-208, Table-4. The diffraction peaks shift to higher angles with Ga doping reveals that the unit cell is shrunken due to decreased 'd' and attributed to that Ga atoms enter the unit cell of the detached ingots In-Ga-Sb matrix. A slight excess of Sb element forming the GaSb second phase at the grain boundary [22] is benefit to reduce the thermal conductivity [23]. Entire detached crystal diffraction angle was increased by decreased 'd' value

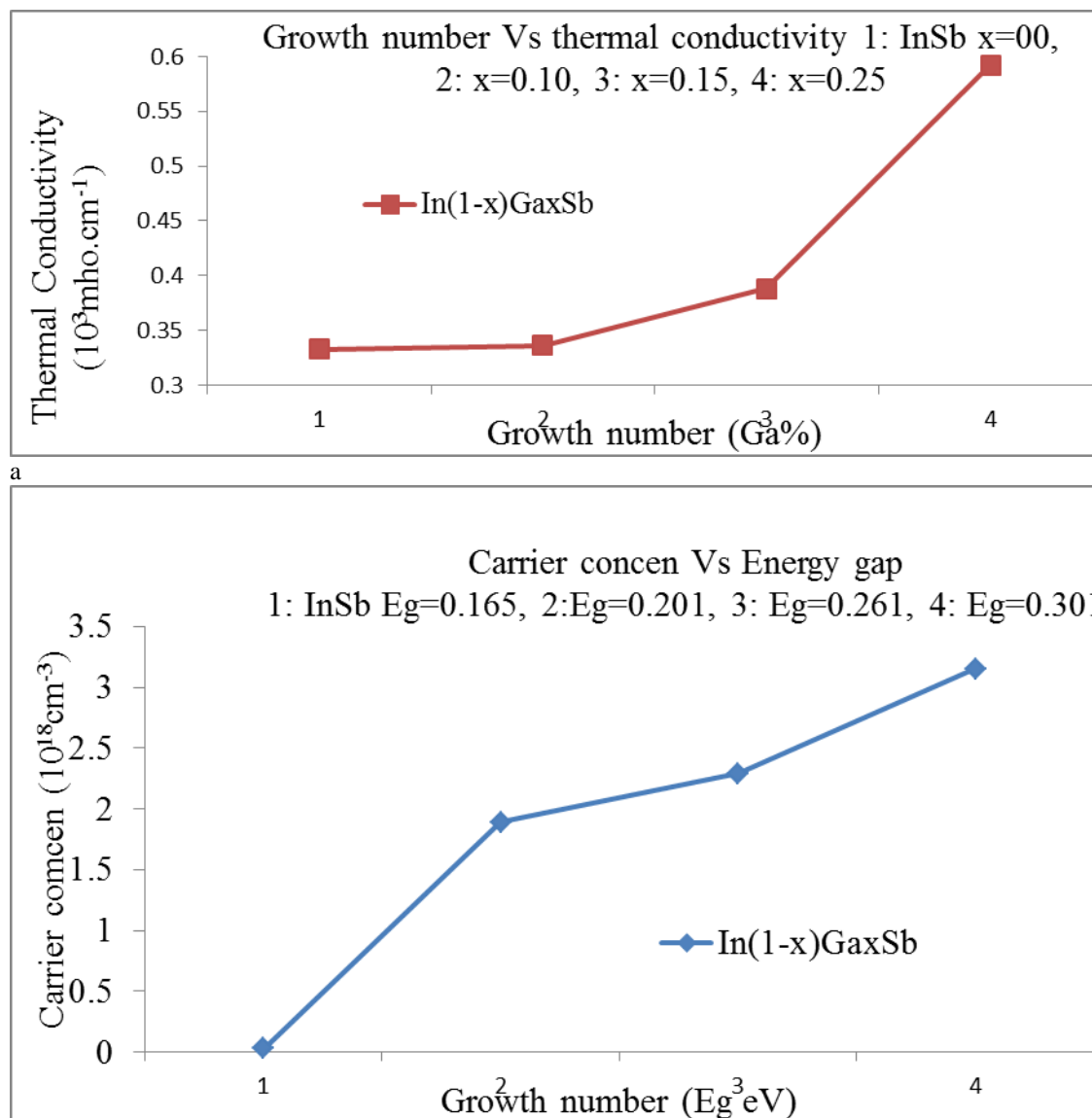


Figure-6 the graph of a) growth number \Ga% Vs Thermal conductivity, b) the growth number energy Vs carrier concentration

corresponds to the increased the full width at half maximum (FWHM). Diffraction peak width was increased with decreased peak intensity, and the increased dislocations density, segregation and defect density. The $\text{In}_{(1-x)}\text{Ga}_x\text{Sb}$ ingots unveil the crystallinity by increasing native acceptor in binary InSb, but it associated with the phase transformation and orientation of the atoms. The structural parameters for $\text{In}_{(1-x)}\text{Ga}_x\text{Sb}$ have matching between the InSb and GaSb crystals [33-37] is a good crystalline quality of the detached crystals by VDS-process XRD patterns displays the $\text{In}_{(1-x)}\text{Ga}_x\text{Sb}$ is well indexed to InSb; the peaks of Ga-doped samples locate between the peaks of pristine InSb (JCPDS card 06-0208) and the pristine GaSb

((JCPDS card 07-0215), indicating the formation of $\text{In}_{(1-x)}\text{Ga}_x\text{Sb}$ grown ingots. The solubility of Ga for $x < 0.2$, while the shoulders of diffraction peaks for $x > 0.2$, the diffraction peaks from a secondary phase in Fig-3e,f is consistent with [22]. We have several interesting growths observations by VDS-process. The formation of secondary phase becomes noticeable at $x > 0.2$, but the secondary phase is negligible for $x < 0.2$. The grain size of secondary phase is larger. The broadening the XRD peak width is a function 'x', the doping distorted lattice, and the FWHM of (220) peak is confirmed that the adding 'Ga' into InSb substance allowing a larger phase space, which suppresses thermal conductivity (κ_L) and improves the ZT value.

Table-5 The measurement by the Hall-van der Pauw method at 300K of the three In(1-x)GaxSb(x= 0.10, 0.15, 0.25) ingots grown by VDS-process

Growth no-1 In(1-x)GaxSb, x=0.10

Growth Ga =0.1%	InGaSb-1-2	InGaSb -1-6	InGaSb-1-8	InGaSb-1-11
Mobility (cm ² / V.sec)	12410	9566	6239	3270
Resistivity (Ohm-cm)	2.98x10 ⁻³	5.14x10 ⁻³	6.98x10 ⁻³	3.16x10 ⁻⁴
Carrier Con (cm ⁻³)	1.89x10 ¹⁸	1.27x10 ¹⁸	1.44x10 ¹⁸	6.05x10 ¹⁸
Hall Coeff cm ³ / Coul	-3.58	-4.92	-4.36	-1.03

Growth no-2, In(1-x)GaxSb, x=0.15

Growth In=0.15%	InGaSb -2-2	InGaSb -2-5	InGaSb -2-13	InGaSb -2-15
Mobility (cm ² / V.sec)	9001	4128	2925	1892
Resistivity (Ohm-cm)	2.58x10 ⁻³	1.34x10 ⁻³	3.28x10 ⁻³	4.78x10 ⁻³
Carrier Con (cm ⁻³)	2.29x10 ¹⁸	4.91x10 ¹⁸	5.76x10 ¹⁸	8.68x10 ¹⁸
Hall Coeff cm ³ / Coulo	-3.02	-3.08	-0.91	-0.41

Growth no. 3 In(1-x)GaxSb, x=0.25

Growth In=0.25%	InGaSb-3-01	InGaSb-3-4	InGaSb-3-7	InGaSb-3-11
Mobility (cm ² / V.sec)	2436	718	582	637
Resistivity (Ohm-cm)	1.69x10 ⁻³	3.10x10 ⁻³	6.42x10 ⁻³	5.5x10 ⁻³
Carrier Con (cm ⁻³)	3.15x10 ¹⁸	2.86x10 ¹⁸	1.67x10 ¹⁸	1.78x10 ¹⁸
Hall Coeff cm ³ / Coulo	-1.47	+2.78	+3.74	+3.38

3.5 Electrical measurement

Hall-van der Pauw measurements, the substrates were selected from the middle section of the entire detached In(1-x)GaxSbingots. The majority carriers are electrons, thus n-type conducted. The electrical resistivity is a function of the charge density of the majority carriers and the mobility, i.e. resistivity $\rho = 1 / e n_e \mu_e$, where e , n_e and μ_e represent the electron charge, electron density, and electron mobility. The resistivity is inversely proportional to carrier density and electron mobility. The Hall result in Table-5 contributes that

the reduced electron mobility than the pristine InSb (6.05x10⁴cm²/V.sec), ~1.24x10⁴cm²/V.sec, ~9.0x10³cm²/V.sec, and ~2.44x10³cm²/V.sec for the In_{0.9}Ga_{0.1}Sb, In_{0.85}Ga_{0.15}Sb, and In_{0.75}Ga_{0.25}Sb crystal respectively. The carrier mobility and concentration in detached growth was influenced by the grain size effect by lower variation in mobility than the carrier concentration. The free carrier concentration of In(1-x)GaxSb increased two orders of magnitude with the binary InSb, while mobility decreases by one order, it attributes dependence on changes in atomic composition, but not in crystal structure. The 'Ga' dopant as isoelectric for 'In' could abrupt decrease of

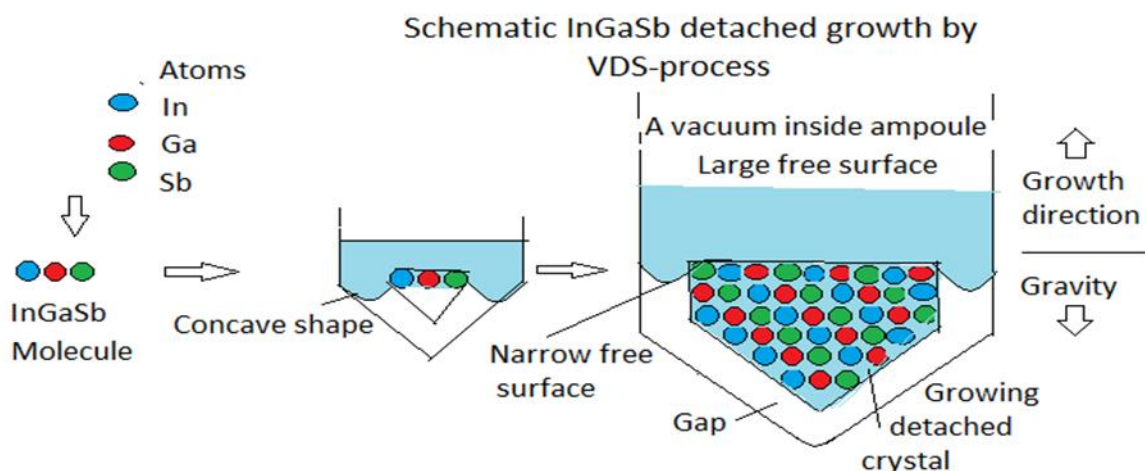


Figure-7 the schematic growth process of the Ga(1-X).InXSb crystal at the atomic level by VDS-process.

the carrier mobility and two order increasing in carrier concentration of the ternary $\text{In}(1-x)\text{Ga}x\text{Sb}$ crystals, which increased the native defect such as vacancy (V_{In} , $V_{\text{In}}V_{\text{Sb}}$, V_{Sb}), antisites (In_{Sb} , Sb_{In}) twin lamella and grain boundaries. The 'Ga' and 'In' occurs in the same lattice position (different lattice), then the ternary compounds $\text{In}(1-x)\text{Ga}x\text{Sb}$ easily grow by changing composition % of 'Ga'. The 'Ga' is an isoelectronic charge carriers doping, thus changes the electrical properties by marginally reducing crystallinity. The reduction in mobility by indium sites and valence sites are close of the atomic radius of 'Ga'. Addition, the 'InSb' doped crystal has non-uniform interface shape due to the increased defect and micro-segregation decreasing the transport properties of $\text{In}(1-x)\text{Ga}x\text{Sb}$ crystals due to stress. The point defects, the isoelectronic dopants, cationic vacancies, and anionic vacancies may scatter short wavelength phonons by minimizing the carrier mobility. The $\text{In}(1-x)\text{Ga}x\text{Sb}$ ($x < 0.2$), the isoelectronic 'Ga' doping simultaneously reduced the lattice thermal conductivity without decreased the carrier mobility, which is important effect of entire detached growth. The high carrier concentration of $1.89-8.6810^{18}\text{cm}^{-3}$ is two orders higher than the pristine InSb ($3.8 \times 10^{16}\text{cm}^{-3}$). The experimental measured carrier concentration is due to the compensation effect of cationic vacancies. The vacancies compensate the excessive electrons result in the nearly unchanged carrier concentration, as shown in Table-5.

3.6 Energy gap

The pseudo-binary and highly mismatched alloys (HMAs) used for the modifications in electronic band structures is important contribution in developing TE materials, with the different approaches, viz. the doping, the microstructure growth and band structure engineering [18-25]. Therefore, the semiconductor crystal is an opportunities for tailoring the physical properties among isoelectronic matches properties for electronic and optoelectronic [24]. The 'Ga' doped $\text{In}(1-x)\text{Ga}x\text{Sb}$ crystals, the energy gap ('Eg') was measured by Hall-van der Pauw geometry at 300K Table-3 and Fig-5, is consistence with [24]. The mobility (μ), the charge carrier concentration (n), the resistivity (ρ) and energy gap ('Eg') are shown in Table-4. The entire detached $\text{In}(1-x)\text{Ga}x\text{Sb}$ crystal reveals the n-type properties for $x < 0.2$ and good for TE application. The effective acceptor concentration of 'Ga' increases with the increase in 'Eg' in n-type-region; the band gap energy increases from 0.16eV of pristine InSb to varying band gap of $\text{In}(1-x)\text{Ga}x\text{Sb}$ Table-3. Effective charge density state of an acceptor increases in ternary $\text{In}(1-x)\text{Ga}x\text{Sb}$, thus

Fermi level shifts below the valence band energy level (E_g). However, 'InSb' composition further decreases by increasing the 'Ga' composition % 'x'. Fermi level shifts further below the band gap energy level E_{Obs} (maximum shift) by the filled effective acceptor charge carriers. A transition from E_{Obs} to the conduction band energy level required large energy ($E_g < E_{\text{Obs}}$), and $E_g = E_{\text{Obs}} - (E_U - E_{\text{BM}})$. The shift is inversely proportional to effective mass by Burstein-Mass equation (BM). While, the log of alpha v/s energy, the reciprocal of the slope is Urbach Energy $\ln\alpha = \ln(\alpha_0) - [(E_g - E_0)/E_U]$. The quality crystal growth of $\text{In}(1-x)\text{Ga}x\text{Sb}$ crystal resulted by detachment [34-48]. Band gap energies modified by varying the composition 'x' to tailor the forbidden gaps for the long-wavelength infrared, Table-3

3.7 Thermoelectric properties

InSb-based crystals are not promising thermoelectric (TE) materials as it has high thermal conductivity [18]. The effort was to control growth of the microstructure, dislocation in perfect single crystal of the binary InSb and decrease the lattice thermal conductivity. The defects growth in InSb matrix such as the eutectic growth, native defects (vacancy, antisite) and micro-inclusions reduces the lattice thermal conductivity. Thus, it is necessary to develop InSb growth scheme to reduce the lattice thermal conductivity without deteriorating the electrical properties. We studied the detached growth by VDS-process as a new approach. The Ga doping in InSb introduces the native defects, vacancy and antisite by the compositional segregation, which can serve as phonon scattering centers. The 'Ga' as isoelectronic substitution for 'In' could acts as scatterer of the short-wavelength phonons and reduce the lattice thermal conductivity; may weaken influence or enhance the electron transport properties by the complex effect on phonon scattering [12]. III-V compounds with the zinc blende structure have high carrier mobility and good power factors by crystal and electronic structure. Experimental results showed Ga into InSb and In into GaSb, the lattice thermal conductivity reduces and increases a ZT value [19-21]. The electrical resistivity affected by point defects and the Seebeck coefficient into electricity. The dimensionless ZT is given by $ZT = S^2\sigma T/\kappa$, where S is the Seebeck coefficient, σ is the electrical conductivity, κ is the thermal conductivity, and T is the temperature [22-25]. The carrier concentration 'n' was by 'n' = $-1/eRH$, where RH is the Hall coefficient. The TE-based materials, the indium antimonide (InSb) is useful as reason i) the constituent elements of InSb based TE material are plenty in earth. ii) the high

electron mobility of the InSb has high material parameter $\beta = (m^*/m_0)^3 / 2\mu\kappa$, could give high ZT [12], where m^* is the carrier effective mass, m_0 is the free electron mass, μ is the carrier mobility and $\kappa = (\kappa_E + \kappa_L)$, κ_L is the lattice thermal conductivity, and κ_E is the thermal of carrier concentration. However, the high lattice thermal conductivity (κ_L) and low mobility is a constraint for TE property of binary InSb compound. To solve this problem, we have doped Ga into InSb and systematically analyzed the effect of Ga alloying on the properties such as the Seebeck coefficient, electrical conductivity (κ_e) and lattice thermal conductivity (κ_L) of InSb. Ga alloying reduced the lattice thermal conductivity (κ_L) and optimized reduction in the mobility of InSb. The properties have been analyzed of Ga doping in $\text{In}_{(1-x)}\text{Ga}_x\text{Sb}$ ($x=0.1, 0.15, 0.25$) crystal at RT. The increase in Ga doping increases 'Eg' Fig-5, the thermal conductivity increases with the increase in Ga% Fig-6a, $\text{In}_{(1-x)}\text{Ga}_x\text{Sb}$ growth, Ga doped and Sb rich forms the second phase of GaSb at grain boundaries, which reduces the thermal conductivity Fig-3. The doping increase carrier concentration (Table-5) by controlling the bipolar effect and enhance in power factor [22]. The InSb based TE materials are attractive in future large-scale commercial application in mid-temperature thermoelectric power generation. The carrier concentration increases with the increase in energy gap Fig-6b. The improvement in the TE of $\text{In}_{(1-x)}\text{Ga}_x\text{Sb}$ due to the point defects and composition segregations to enhance the thermoelectric (TE) properties of crystalline materials, the VDS experimental defect engineering study is under process.

3.8 The principle of entire detached growth in VDS-process

The concept of the growth process by VDS-process in [44-46] is similar as shown schematically in Fig-7. In brief, the source materials Indium (In), Gallium (Ga) and Antimonide (Sb) atoms are shown in solid circles (In-blue, Ga- red, Sb-green), and its InGaSb molecule formation process in Fig-7a. The strong bond of the In-Ga-Sb atoms exists, and then InGaSb molecule forms under the optimum growth Fig-7b. A tiny melt drop of homogeneous melt emerges 3-D structure of the melt by binding energy of In-Ga-Sb, Fig-7c. The entire dangling melt drop detaches into conical shape of an ampoule due to the molecular binding and bonding energy. The dangling melt drop forms away from the inner wall of an ampoule. The growth set up serendipitously as the apparition of a gap, and forms solid by the slow freezing of the solidification or crystallization process, Fig-7. It spontaneously promotes the

concave meniscus and concave C/M interface and concave solidified tip (seed) is shown in Fig-7c, the schematically in Fig-1d, and actual shape by grown ingots in Fig-2. The homogeneous and the chemically uniform structure of the melt freezes, hence the single crystal grows. The spontaneous preferential growth self-selected (022) direction of the crystalline structure grows. The entire detached crystal growth length increases continuously vertical direction with the time, schematically Fig-1d. Melt was formed concave meniscus shape with the inner wall of an ampoule with growing crystal, i.e. blue curve shape. The concave meniscus and concave crystal-melt interface are observed from the melt large free surface (a vacuum). The self-seed growth and the self-stabilization of the pressure developed. The non-steady growth presents, the entire detached growths by VDS-process, might be the capillary stability and the surface features close to detached crystal growth in space [28-33].

II. CONCLUSION

First time, the 'Ga' doped three $\text{In}_{(1-x)}\text{Ga}_x\text{Sb}$ ($x=0.10, 0.15, 0.25$) entire detached crystals were grown. The $\text{In}_{(1-x)}\text{Ga}_x\text{Sb}$ detached bulk crystals characterization showed the lower crystalline quality with binary. Doping of Ga in InSb changes in binary InSb crystals as the decreased carrier mobility from $\sim 6.0 \times 10^4 \text{ cm}^2/\text{V}\cdot\text{sec}$ to 1.241×10^4 , 9.01×10^3 , and $2.436 \times 10^3 \text{ cm}^2/\text{V}\cdot\text{sec}$, the marginal reduction in resistivity ($3.0 \times 10^{-3} \Omega\cdot\text{cm}$), two fold increase in carrier concentration from $\sim 3.8 \times 10^{16} \text{ cm}^{-3}$ (InSb) to ~ 1.27 , 4.91 and $2.86 \times 10^{18} \text{ cm}^{-3}$, and increase in dislocation density from $\sim 962 \text{ cm}^{-2}$ in InSb to ~ 1.21 , 6.94 and $9.93 \times 10^3 \text{ cm}^{-2}$. The higher dislocation density, the lower resistivity and the higher mobility are measured, it reveals the crystalline growth of the ternary entire detached $\text{In}_{(1-x)}\text{Ga}_x\text{Sb}$ crystals by VDS-process, and the preferred (022) direction. The controlled band gap, optoelectronic, electrical and structural properties of the $\text{In}_{(1-x)}\text{Ga}_x\text{Sb}$ crystal grown by the novel VDS-process are confirmed, and nearby to the detached crystal growth in space..

REFERENCES

- [1]. I. Vurgaftman, Meyer, J. & Ram-Mohan, L., *J. Appl. Phys.* 89, 5815–5875 (2001)
- [2]. Del Alamo, J. A., *Nature* 479, 317–323 (2011)
- [3]. Ma, Z Qin, G Xie, L Qian, D Tang *Appl. Phys. Rev.* 6, (2019) 021317
- [4]. Ebnalwaled, A.A. Duffar, T., Sylla, L. *Crystal Research Techno* 48(4), (2013), 236

- [5]. Buckeridge, J., Veal, T.D., Catlow, C.R.A., Scanlon, D.O. *Physi Review B*100(3), (2019), 035207
- [6]. Flores Mena, J.E., Castillo Ojeda, R., Díaz Reyes, J., *J Mechanics* 1616 (3) (2014) 1
- [7]. Gorji Ghalamestani, S., Ek, M., Ganjipour, B., Thelander, C., Johansson, J., Caroff, P., Dick, K.A *Nano Letters* 12(9,12) (2012) 4914-4919
- [8]. Jianbin Wang, Liya L. Regel, William R. Wilcox, *J Crystal Growth* 260 (2004) 59
- [9]. Lamine Sylla, Thierry Duffar, *J Crystal Growth* 324 (2011) 53–62
- [10]. Raquel Giulian, Charles A. Bolzan, Leandro T. Rossetto, Antônio Marcos H. de Andrade, Júlio R. Schoffen, Leandro L. Araujo, Henri I. Boudinov, *Thin Solid Films* 709 (2020) 138213
- [11]. H. Bekhouche, A. Gueddim, N. Bouarissa, N. Messikine, *Chine J Physics* 65 (2020) 146–152
- [12]. Zhengliang Dua, Xiaolu Chena, Junhao Zhuh, Jiaolin Cuia, *Current Appl Physics* 18 (2018) 893–897
- [13]. Jihye Kang, Jung-Hyuk Koh, *Ceramics International* 46 (2020) 10603–10609
- [14]. Akant Sagar Sharma, Subhasis Dasa, b, S. Dhara, *J Crystal Growth* 545 (2020) 125739
- [15]. Beo Deul Ryu, Min Han, Kang Bok Ko, Tran Viet Cuong, Chang-Hyun Limd, Gun Hee Lee, Chang-Hee Hong
- [16]. Y.J. Jin, X.E. Zheng, S.J. Gon, C. Ke, M.Q. Xiao, B. Ling, S.Y. Yu, D.H. Zhang, *J Alloys and Compounds* 823 (2020) 153758
- [17]. Famin Liu*, Lide Zhang, *J Crystal Growth* 204 (1999) 19}23
- [18]. Zhang, Q., Xiong, Z., Jiang, J.a, Li, W., Xu, G., Bai, S., Cui, P., Chen, L. J *Materials Chemistry*21(33), (2011) 12398
- [19]. Kumar, V.N., Hayakawa, Y., Udono, H., Inatomi, Y. *Inorganic Chem* 58(17) (2019) 11579-11588
- [20]. Nirmal Kumar, V. Arivanandan, M. Koyoma, T. Udono, H.d, Inatomi, Y., Hayakawa, Y. *Appl Physics A: Mater Sci Proce* 122(10) (2016) 885
- [21]. Du, Z., Yan, M., Zhu, J. *Materials Research Express* 5(10), (2018) 106301
- [22]. Jing Jiang, Rui Zhang, Chengcheng Yang, Yi Niu, Ting Zhou, Yan Pan, Chao Wang, *J Materiomics* 6 (2020) 240e247
- [23]. S. AlFaify, Bakhtiar Ul Haq, R. Ahmed, Faheem K. Butt M.M. Alsardia, *J Alloys and Compounds* 739 (2018) 380e387
- [24]. Huan Tan, Bin Zhang, Guoyu Wang, Yongjin Chen, Xingchen Shen, Lijie Guo, Xiaodong Han, Xu Lu Xiaoyuan Zhou, *J Alloys Compounds* 774 (2019) 129e136
- [25]. Zhengliang Dua, Jian Heb, Xiaolu Chena, Mengyi Yana, Junhao Zhuc, Yamei Liub *Intermetallics* 112 (2019)106528
- [26]. Y Inatomi, K Sakata, M Arivanandhan, G Rajesh, V Nirmal Kumar, T Koyama, Y Momose, T Ozawa, Y Okano, Y Hayakawa, *npj Microgravity* 1 (2015) 15011
- [27]. J Yu, Y, V N Kumar, Y Hayakawa, Yi Okano, M Arivanandhan, Y Momose, X Pan, Y Liu, X Zhang, X Luo, *npj Microgravity* 5 (2019) 8
- [28]. Jianding Yu, Yuko Inatomi, Velu Nirmal Kumar, Y Hayakawa5, Y Okano, M Arivanandhan, Y Momose5, X Pan1, Y Liu1, X Zhang X Lu, *npj Microgravity* 5 (2019):8
- [29]. Y Inatomi, K Sakata, M Arivanandhan, G Rajesh, V Nirmal Kumar, T Koyama, Y Momose, T Ozawa, Y Okano, Y Hayakawa, *npj Microgravity*, 1 (2015) 15011
- [30]. Yu, J. Liu, Y, Pan, X, Zhao, H, Kumar, V.N, Arivanandhan, M., Momose, Y, Hayakawa, Y, Zhang, X, Luo, X, Okano, Y, Inatomi, Y. *Microg Sci Techno* 28(2) (2016) 143-154
- [31]. Hongxiang Jiang, Shixin Li1, Lili Zhang, Jie He, Jiuzhou Zhao, *npj Microgravity* 5 (2019) 26
- [32]. Xinghong Luo, Yaya Wang, Yang Li *npj Microgravity* (2019) 5:23
- [33]. Gadkari D.B., *J Chemi Chemi Enginee* 6,2012 65,
- [34]. Gadkari D.B., *J Chemi Chemi Enginee* 6,2012 250
- [35]. Gadkari Dattatray, *J Materi Sci Engin A3* 2(9),2012, 593
- [36]. Gadkari D.B., *Ameri Insti Phys, Conf Pro* 1512,2013 856
- [37]. Gadkari D.B., *J Materi Sci Engineeg* A3(5), (2013),338
- [38]. D.B. Gadkari, B.M. Arora, *Material Chemistry and Physics* 139 (2013) 375
- [39]. D.B.Gadkari, *Interna J. Sci Res Publ* 4 (2014) 1
- [40]. Dattatray Gadkari, *Intern J Enginee Appl Sci (IJEAS)* 2(4) (2015) 39
- [41]. D. Gadkari, D. Maske, M. Deshpande, B Arora, *Inten. J. Innov. Resea Sci. Eng* 5(2) (2016) 2092
- [42]. Dattatray Gadkari, *J Electro Commu Engineering (IOSR-JECE)* 12(4) IV (2017), 51-58
- [43]. Dattatray Gadkari, *J Electro Commu Engineering (IOSR-JECE)* 13(3) (2018), 21-31

- [44]. Dattatray Gadkari, *Int J Eng Res App* 8(4) (2019) 01-19
- [45]. D B Gadkari, *Int J Eng Res App* 10(5) (2020) 7-20
- [46]. D B Gadkari, *Int J Eng Res App* 10(9) (2020) 5-19
- [47]. D Maske, M Deshpande, D Gadkari, *J Nano and Electronis Physics*12 (2) (2020)2012

awards/medals/certificates from academic societies such as Materials Chemistry and Physics, Indian Association of Crystal Growth, ASM International India Chapter, Shivaji University Kolhapur India, Several Research Institutes / Colleges within India and also from abroad.



Dr D B Gadkari, received B Sc (Physics) degree (1974) from Shivaji University, Kolhapur and M.Sc. degree in Physics from Bombay University (1976), and then University of Mumbai confirmed M Phil (1986) and Ph. D. under UGC-FIP (1998). He joined Mithibai College, Mumbai India (Nov-1976) as a Asst Prof, then HOD- Physics (2000-14), Asso prof (2006-2014), Vice-Principal (2010-2013) and Principal-I/C (2013-2014). He was Adjunct Research Guide-Faculty of Science: University of Mumbai (2014-2017), was at University of Mumbai- Board of Study Member in Physics (2005-2014), Faculty of Science Member (2005-2014); Board of Study Member in Bio-Physics (2010-2014). From June 1, 2017, Dr Gadkari is Freelance research and Consultant: Crystal Growth and Crystal Technology (Crystal Growth, Material Science, Solid State Physics and Physics of devices). He has been published 52 articles in referred journals and in the 32proceedings. The single crystal growth a new growth process - vertical directional solidification (VDS) has been developed successfully, and which shows the detached phenomenon concept for Sb-based (III-V) quality bulk crystals in a terrestrial lab (on Earth). These crystals showed highest physical properties for crystals grown ever, while crystals are analogous to the crystal grown in microgravity. Member of professional International and National research journals. He has successfully completed Research projects (nine) sponsored by government of India and parent institute (SVKM). Indian patents in his name for the detached crystal growth by VDS in the terrestrial lab. This approach has opened a new area for high quality entire detached single crystal growth. He has received several kinds of

D. B. Gadkari. "Study of the Ga doped $\text{In}_{(1-X)}\text{GaXSb}_x$ compositional, structural, electrical, and the microstructures process." *International Journal of Engineering Research and Applications* (10), 2020, pp 35-51.